Chemical Science

ROYAL SOCIETY OF CHEMISTRY

EDGE ARTICLE

View Article Online
View Journal | View Issue

Cite this: *Chem. Sci.*, 2024, **15**, 14425

All publication charges for this article have been paid for by the Royal Society of Chemistry

Unlocking the potential: strategic synthesis of a previously predicted pyrazolate-based stable MOF with unique clusters and high catalytic activity†

Xiang-Yu Li, Yan-Long Zhao, Su-Nan Chen, Kecheng Wang,* Shengjun Wang, Lin-Hua Xie * and Jian-Rong Li *

The metal–organic framework (MOF) constructed from $[Co_4Pz_8]$ clusters (Pz = pyrazolate) and 1,3,5-tris(pyrazolate-4-yl) benzene (BTP^{3-}) ligands was structurally predicted many years ago, and expected to be a promising candidate for various applications owing to its unique clusters and highly open 3D framework structure. However, this MOF has not been experimentally prepared yet, despite extensive efforts were made. In this work, we present the successful construction of this MOF, hereinafter referred to as **BUT-124(Co)**, by adopting a two-step synthesis strategy, involving the initial construction of a template framework (**BUT-124(Cd)**) followed by a post-synthetic metal metathesis process. The effects of various cobalt sources and solvents were systematically investigated, and an innovative stepwise metathesis strategy was employed to optimize the exchange rates and the porosity of the material. **BUT-124(Co)** demonstrates high catalytic activity in the oxygen evolution reaction (OER), achieving a competitive performance with an overpotential of 393 mV at a current density of 10 mA cm^{-2}, and also affords remarkable long-term stability during potentiostatic electrolysis in 1 M KOH solution, surpassing the durability of many benchmark catalysts. This work not only introduces a novel MOF material with promising properties but also exemplifies a strategic synthesis approach for pyrazolate-based MOFs, paving the way for advancements in diverse application fields.

Received 17th June 2024
Accepted 7th August 2024

DOI: 10.1039/d4sc03973d

rsc.li/chemical-science

Metal–organic frameworks (MOFs) are an emerging class of crystalline porous materials assembled with metal ions/clusters and organic linkers.[1–3] In the last two decades, the significant potential of MOFs in gas separation/storage,[4–7] catalysis[8–10] and other applications[11–13] has been extensively explored and solidly demonstrated. Among the various advantages of MOFs, the structural diversity and tunability are the most important ones that contribute to the excellent performance of these materials in many different applications. Particularly, the transition metal ions inside the metal clusters of MOFs can display unique coordination environments that are rarely observed within traditional organometallic compounds or small molecule complexes.[14–16] As a result, the metal centers of MOFs could exhibit special chemical reactivity.[17,18]

Although several strategies have been developed to facilitate the construction of MOFs with targeted structures, in some cases it is still highly challenging to obtain desired MOFs through direct synthesis methods. To date, the crystal growth process remains a "black box", and it can hardly be decoded even by the state-of-art technologies, which makes the adjustment of MOFs' synthesis conditions very tricky in many cases. Therefore, besides direct synthesis,[19] some other methods have also been explored to promote the formation of targeted MOFs, such as post-synthetic modification,[20–22] and solvent-assisted metal metathesis.[23–25]

Pyrazolate-based MOFs (Pz-MOFs) are a special type of MOFs constructed from pyrazolate ligands and transition metal ions. Besides their high base stability, Pz-MOFs offer several advantages over carboxylate-based MOFs.[26] Since the N atoms of pyrazolate groups act as stronger σ donors, the electron densities of transition metal ions in Pz-MOFs could be higher. Moreover, the transition metal ions can form distinctive clusters and display unique coordination environments in Pz-MOFs, which could not be obtained in carboxylate-based MOFs. These factors enable the metal sites in Pz-MOFs to exhibit special chemical reactivity, and endow the materials with great potential as catalysts or sorbents.[27]

However, compared with carboxylate-based MOFs, it is more challenging to develop effective strategies to modulate the crystal growth of Pz-MOFs.[28–30] This could be due to the

Beijing Key Laboratory for Green Catalysis and Separation, Department of Chemical Engineering, College of Materials Science and Engineering, Beijing University of Technology, Beijing 100124, P. R. China. E-mail: kcwang@bjut.edu.cn; xielinhua@bjut.edu.cn; jrli@bjut.edu.cn

† Electronic supplementary information (ESI) available. See DOI: https://doi.org/10.1039/d4sc03973d

difficulties in regulating the nucleation rate and the lack of reversibility inherent in the crystal growth process of these frameworks. As a result, some Pz-MOFs with excellent properties have been predicted, but cannot be successfully obtained. A typical example is **Co-BTP**, which was first simulated and reported by Long's group in 2016.[31] By exploring the adsorption behaviors of its iso-structural MOFs, including **Co-BTTri** and **Co-BDTriP**, Long and co-workers predicted that the open metal sites of **Co-BTP** could serve as very effective capture sites for some gas molecules. Furthermore, the simulation studies also demonstrated the high potential of **Co-BTP** in several electrochemical reactions, such as oxygen evolution reaction (OER).[32] Unfortunately, **Co-BTP** could not be successfully obtained, even extensive efforts have been made to adjust its synthesis conditions. A possible explanation was proposed that, under typical solvothermal conditions, the reaction of Co^{2+} and 1,3,5-tris(1*H*-pyrazol-4-yl)benzene (H_3BTP) prefers to form another phase, which is more thermodynamically favored.[33]

In this work, we report the strategic synthesis of this MOF material through a two-step method. A template framework, **Cd-BTP**, hereinafter referred to as **BUT-124(Cd)**, was synthesized first. Then, the Cd^{2+} ions were exchanged with Co^{2+} by post-synthetic metal metathesis (Scheme 1). There are several advantages to choose Cd^{2+} to construct the template MOF. First, Cd^{2+} could exhibit versatile coordination modes and has the potential to form the targeted [M_4Pz_8] clusters with pyrazolate groups. Moreover, the valence electron configuration of Cd^{2+} is 4d,[10] and no extra crystal field stabilization energy could be provided when Cd^{2+} coordinates with ligands. At the same time, considering that the radius of Cd^{2+} is larger than most divalent metal ions of the first transition series, the coordination bonds between Cd^{2+} and pyrazolate groups would not be very strong, which could provide enough thermodynamic driving force to replace the Cd^{2+} inside the framework with Co^{2+} through metal metathesis. After carefully exploring and optimizing the conditions for the synthesis and metal metathesis of **Cd-BTP**, **Co-BTP** was successfully obtained, namely **BUT-124(Co)**. The chemical stability and electrochemical activity of this material have been investigated. **BUT-124(Co)** showed excellent base resistance that could retain its crystallinity in 1 M KOH solution. Moreover, it exhibited efficient catalytic activity for the OER (with an overpotential of 393 mA at a current density of 10 mA cm^{-2}) and good working stability.

The template MOF **BUT-124(Cd)** was prepared in a 25 mL Teflon-lined reactor under solvothermal reaction conditions at 80 °C (details in the ESI†). The PXRD pattern of **BUT-124(Cd)** was fitted by using the Pawley method.[34] The detailed data are listed in Table S1† and fitted PXRD patterns for the Pawley refinement are shown in Fig. S3.†

The powder X-ray diffraction (PXRD) analyses illustrated that the **BUT-124(Cd)** crystallized in the cubic crystal system, *Pmm* space group, with the *a* axis of 19.506(7) Å, which was obviously larger than that of $Cu_3(BTP)_2$ (18.8070(8) Å).[33] By comparing the calculated PXRD pattern with the experimental one, the result strongly indicated that **BUT-124(Cd)** was isostructural with $Cu_3(BTP)_2$ (Fig. 1). **BUT-124(Cd)** consisted of the [Cd_4Pz_8] cluster and BTP^{3-} ligands, adopting a sodalite (**SOD**) topological structure. In the [Cd_4Pz_8] cluster, each Cd atom was coordinated with four N atoms from the Pz ligands, forming a planar quadrilateral coordination (Scheme 1). The SEM analysis showed that the particles of as-synthesized **BUT-124(Cd)** samples exhibited octahedral morphology with a size of around 50–60 nm (Fig. S2†). A N_2 sorption isotherm of **BUT-124(Cd)** was measured at 77 K (Fig. 2a). The Brunauer–Emmett–Teller (BET) surface area of **BUT-124(Cd)** was calculated to be 1563.6 $m^2 g^{-1}$. And the experimental total pore volume was 0.68 $cm^3 g^{-1}$, which was close to the calculated value of 0.73 $cm^3 g^{-1}$. The stability test of **BUT-124(Cd)** showed that it completely decomposed after being exposed in air for one hour, demonstrating its chemical lability (Fig. 3a).

To obtain the targeted framework of **BUT-124(Co)**, the post-synthetic metal exchange strategy was adopted to treat the as-synthesized **BUT-124(Cd)** sample. At first, we chose $Co(NO_3)_2 \cdot 6H_2O$, $Co(OAc)_2 \cdot 4H_2O$, $CoCl_2 \cdot 6H_2O$ or $Co(ClO_4)_2 \cdot 6H_2O$ as the cobalt source, and acetone, methanol (MeOH), *N*,*N*-

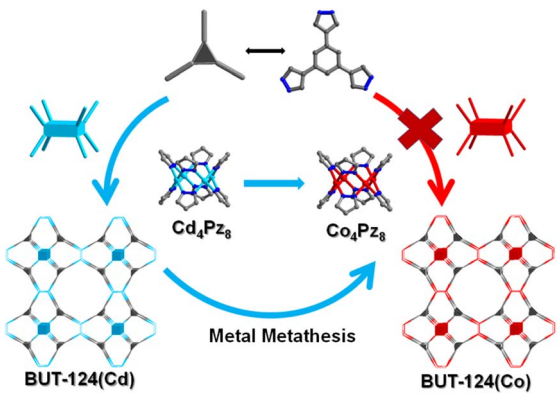

Scheme 1 Two-step synthetic approach to prepare BUT-124(Co) with [Co_4Pz_8] clusters. A Co(II) metal–organic framework BUT-124(Co) was obtained through the metal metathesis of iso-reticular BUT-124(Cd).

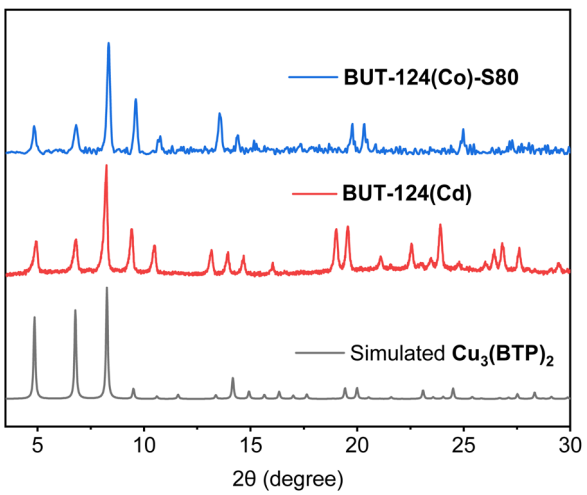

Fig. 1 The experimental PXRD patterns for BUT-124(Cd) and BUT-124(Co)-S80 obtained by metal metathesis and the simulated PXRD patterns for $Cu_3(BTP)_2$.

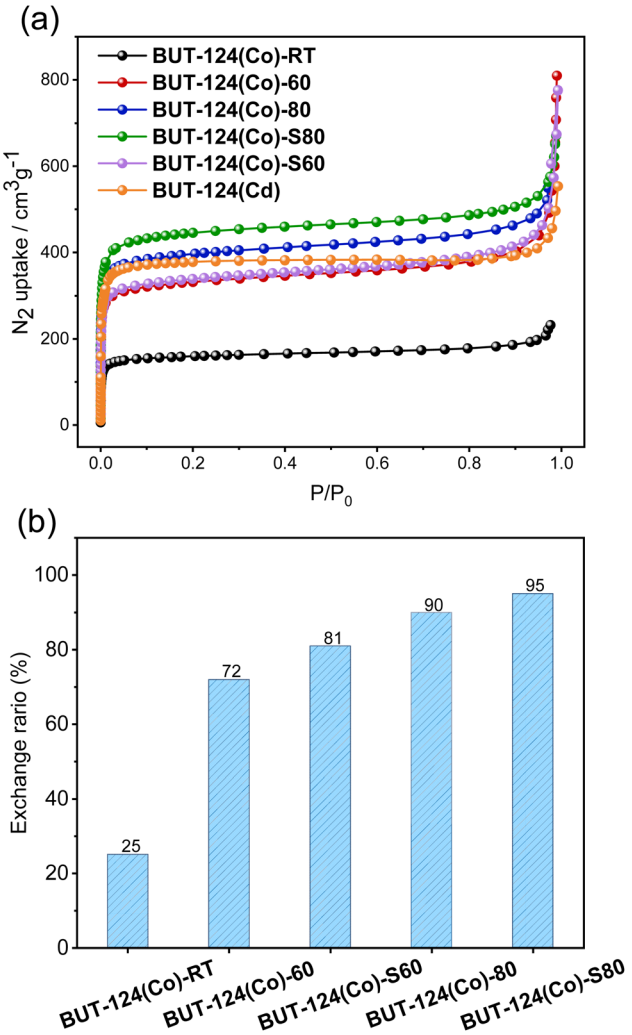

Fig. 2 (a) N_2 sorption isotherms of BUT-124(Co) obtained under different exchange conditions. (b) Bar graphs of the exchange ratio of different BUT-124(Co) samples.

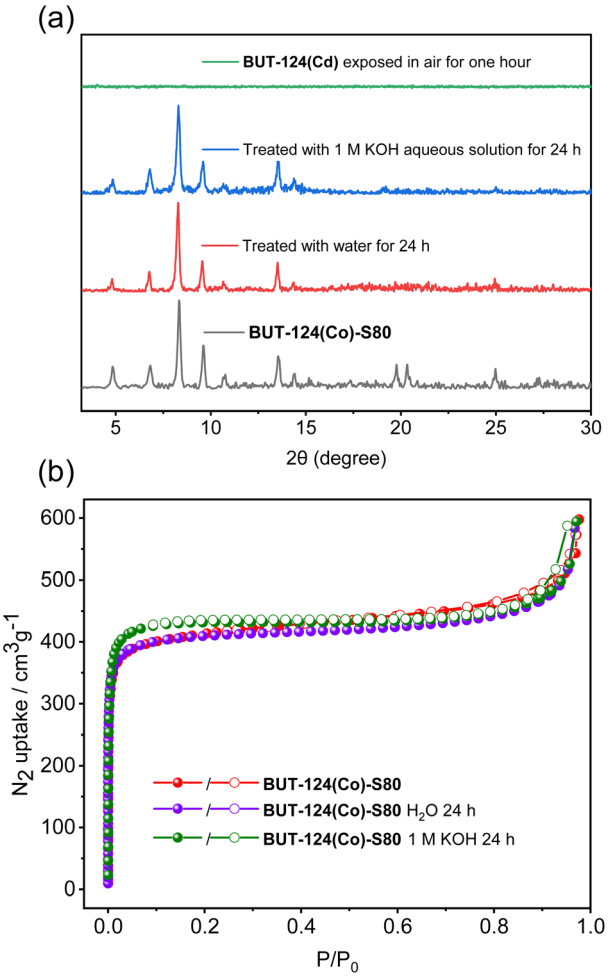

Fig. 3 PXRD patterns (a) and 77 K N_2 sorption isotherms (b) of BUT-124(Co)-S80 samples after being treated under different conditions.

dimethylformamide (DMF) or *N*,*N*-dimethylacetamide (DMA) as the solvent to prepare different solutions with the concentration of 10 mg mL^{-1} (details in Table S2†). Then the as-synthesized **BUT-124(Cd)** samples were immersed in the above-mentioned solutions at room temperature (RT), 60 °C and 80 °C for two days, respectively. The samples were collected and washed with DMA and MeOH for PXRD measurements. The results showed that the samples treated with a DMA solution of $Co(NO_3)_2 \cdot 6H_2O$ retained the best crystallinity, and the colors of the initially white samples changed to dark brown after metal metathesis (Fig. S5†). To investigate the exchange ratios of the three samples at different exchange temperatures, inductively coupled plasma (ICP) analyses of these treated samples were carried out. The exchange ratios of **BUT-124(Co)-RT**, **BUT-124(Co)-60**, and **BUT-124(Co)-80**, which were treated with DMA solutions of $Co(NO_3)_2 \cdot 6H_2O$ at RT, 60 °C and 80 °C, reached 25%, 72% and 90%, respectively (Fig. 2b and Table S3†), indicating that the increase of temperature could promote the metal metathesis process. The permanent porosity of the treated samples has been confirmed by N_2 adsorption measurements at 77 K. The N_2 uptakes of 186 cm^{-3} g^{-1}, 402 cm^{-3} g^{-1} and 463 cm^{-3} g^{-1} were achieved at $P/P_0 = 0.9$ corresponding to intracrystalline pores (Fig. 2a). The experimentally determined porosities of **BUT-124(Co)-RT** and **BUT-124(Co)-60** were obviously lower than the theoretical value (N_2 uptake: 598 cm^3 g^{-1}). Considering the low stability of **BUT-124(Cd)**, it was reasonable to attribute the compromised porosities of the treated samples to the partial degradation of the template framework during the metal metathesis. On one hand, the elevated temperature promoted the metal exchange rate and increased the porosities of the resultant samples. On the other hand, the framework could be easier to get destroyed at an elevated temperature.

To further optimize the metal metathesis conditions, we developed a step-by-step exchange strategy. We first soaked **BUT-124(Cd)** in a 10 mg mL^{-1} DMA solution of $Co(NO_3)_2 \cdot 6H_2O$ at RT for one day, then at 60 °C for another day. The obtained sample was labelled as **BUT-124(Co)-S60**. After further incubating **BUT-124(Co)-S60** in a 10 mg mL^{-1} DMA solution of $Co(NO_3)_2 \cdot 6H_2O$ at 80 °C for one more day, the sample labelled as **BUT-124(Co)-S80** was obtained. The PXRD, nitrogen

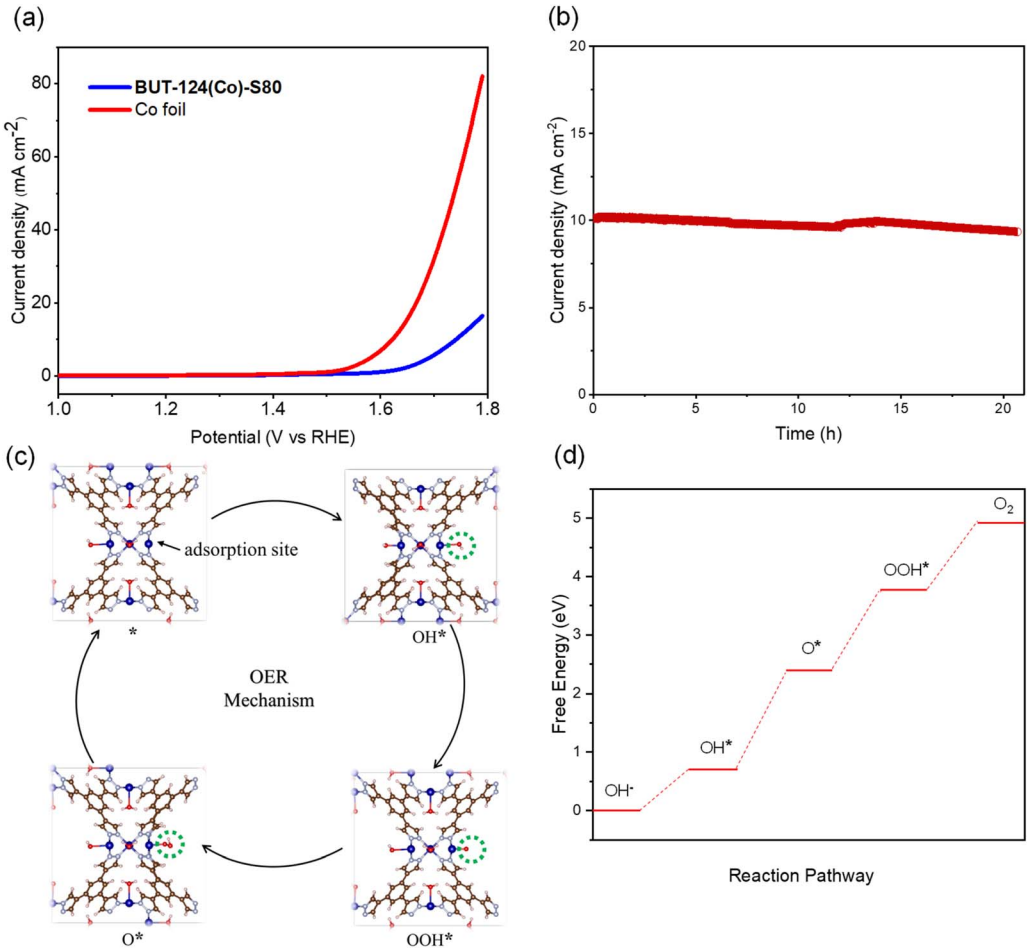

Fig. 4 (a) LSV curves of Co foil and **BUT-124(Co)-S80** in a solution of 1 M KOH. (b) The chronopotentiometry curves of **BUT-124(Co)-S80** at an overpotential of 393 mV in 1 M KOH solution. (c) Schematic illustration of the proposed OER mechanism. Color code: Co, blue; C, brown; N, gray; O, red; H, white. (d) The free energy profile for the OER pathway.

adsorption and ICP of the treated samples were measured. It was found that, with this new strategy, the metal exchange rates of the treated samples were enhanced up to 95% (Fig. 2b and Table S3†), and their porosities were also further improved, while the pore size distribution and PXRD patterns of these materials remained essentially unchanged (Fig. S6†). These results demonstrated that the step-by-step exchange strategy did mitigate the destruction of the parent framework during the exchange process and increase the exchange ratio. Probably, the framework was most sensitive at the initial stage of metal metathesis, and the framework was least destroyed when carrying out the exchange reaction at rt, although the metal exchange rate at RT was low, which resulted in an intermedium phase with pores partially blocked. A gradual lift of the exchange temperature drove completing of the exchange process with framework intact and finally afforded the open framework of **BUT-124(Co)**. After the optimization of metal metathesis conditions, **BUT-124(Co)-S80** was found to be the best-treated sample with the highest metal exchange rate (95%) and porosity (N_2 uptake of 512 $cm^3\ g^{-1}$ at $P/P_0 = 0.9$). It was worth noting that **BUT-124(Co)-S80** exhibited higher porosity than the template MOF **BUT-124(Cd)**, which could be attributed to the well-maintained structure during the metal metathesis and the relatively lower atomic weight of Co^{2+}.

The low stability of **BUT-124(Cd)** would be explained by the weak coordination bonds between Cd^{2+} and pyrazolate groups. The chemical stability of **BUT-124(Co)-S80** was also checked. The samples were treated in liquid water and the aqueous solution of strong basic solutions at RT for 24 h, respectively. The PXRD patterns and N_2 uptakes of all the treated samples remained almost unchanged (Fig. 3, S7 and S8†). And we performed a Pawley fitting analysis on the unit cell of **BUT-124(Co)-S80**. It was found that there is a reduction in the unit cell length for **BUT-124(Co)-S80** when compared to **BUT-124(Cd)** (Fig. S4b and Table S1†). The results demonstrated the significantly improved chemical stability of **BUT-124(Co)-S80** in neutral and basic aqueous solutions, which should be attributed to the formation of stronger coordination bonds between Co^{2+} and pyrazolate groups of the ligands.

To evaluate the thermal stability of the materials, we conducted the TGA (Thermogravimetric Analysis) measurement. The thermogravimetric analysis (TGA) curve indicates that **BUT-**

124(Co)-S80 exhibits higher thermal stability up to approximately 415 °C than **BUT-124(Cd)** (324 °C) (Fig. S9†).

The good base stability of **BUT-124(Co)-S80** and the unique coordination environment of Co^{2+} in the $[Co_4Pz_8]$ cluster encouraged us to explore the potential of this material as a catalyst in the OER. A drop-coating strategy was used to load the active catalyst material on the cobalt foil (details in the ESI†). The linear sweep voltammetry (LSV) method was utilized to examine the OER activity of the **BUT-124(Co)-S80** (Fig. 4a). As a comparison, the blank Co foil was also tested under the same conditions. At a current density of 10 mA cm^{-2}, the overpotential of the electrode loaded with **BUT-124(Co)-S80** was measured to be 393 mV (Fig. 4a), which outperforms most of the reported MOFs (Table S4†). The Co^{2+}/Co^{3+} redox couple exhibits distinct peaks within the potential range of 1.123 to 1.143 V *vs.* RHE (Fig. S23a†). The redox peak potentials observed for Co^{2+}/Co^{3+} in **BUT-124(Co)-S80** are notably lower than those reported for $Co(OH)_2$/CoOOH, as depicted in Fig. S23b.† This reduction in redox potential suggests that the N-coordinated sites significantly alter the electrochemical properties of Co. Additionally, the quantity of Co^{2+}/Co^{3+} sites was determined by integrating the area under the corresponding reduction and oxidation peaks, as detailed in Fig. S23c–e.†[35] The result indicates that the ratio of Co^{2+}/Co^{3+} is about 62.3%.

To understand the relationship between the $[Co_4Pz_8]$ metal cluster and the properties, we performed the density functional theory (DFT) calculations to determine the Gibbs free energy of the various intermediate species involved in the electrochemical OER. We considered the unsaturated metal site as the OER-active site, named the Co-site (Fig. 4c). The binding energies of OH*, O*, and OOH* intermediate species involved in the OER process were calculated for these active sites. Fig. 4d shows the Gibbs free energy of the formation for each elementary step of the OER computed for the four-electron reaction pathway. $OH^* + OH^- \rightarrow O^* + e^- + H_2O$ was found to be the rate-determining step.

The long-term durability is also a critical factor to evaluate the performance of OER catalysts. Thus, the working stability of **BUT-124(Co)-S80** for catalyzing the OER was tested by potentiostatic electrolysis in 1 M KOH solution. The *I–t* curve (Fig. 4b) demonstrated that no significant attenuation of the catalytic current density was observed after 20 h of continuous measurement, which is superior to the durability of IrO_2/C under the same conditions.[36]

Conclusions

In summary, by adopting a two-step synthesis strategy, we successfully obtained a novel Pz-MOF constructed with the $[Co_4Pz_8]$ cluster and BTP^{3-}, which was previously predicted but could not be experimentally prepared by direct synthetic methods. A labile template framework (**BUT-124(Cd)**) was first constructed followed by a post-synthetic metal exchange process to yield the targeted structure of **BUT-124(Co)**. Moreover, a stepwise metal metathesis strategy was developed to increase the metal exchange ratio (up to 95%) and maximize the preservation of the structural integrity of the material at the same time. **BUT-124(Co)** exhibited dramatically increased robustness, especially in basic aqueous solutions. In virtue of its high chemical stability and the special coordination environment of Co^{2+} in **BUT-124(Co)**, this material displayed high activity and working durability as the catalyst for the OER. This work illustrated a practical example to obtain MOFs with desired structures by exploring new synthesis strategies, which could shed light on the further development of novel Pz-MOFs with good performance in different application fields.

Data availability

The data supporting this article have been included as part of the ESI.†

Author contributions

Original idea was conceived by J.-R. Li and K. Wang; experiments and data analysis were performed by X.-Y. Li, K. Wang and L.-H. Xie; structural characterization was performed by Y.-L. Zhao and S.-N. Chen; ligand synthesis was performed by S. Wang. All the authors participated in the preparation of the manuscript.

Conflicts of interest

There are no conflicts to declare.

Acknowledgements

We acknowledge financial support from the National Natural Science Foundation of China (no. 22225803 and 22038001) and Beijing Natural Science Foundation (no. Z230023 and 2242002).

Notes and references

1 H. C. Zhou, J. R. Long and O. M. Yaghi, *Chem. Rev.*, 2012, **112**, 673–674.
2 J. Canivet, A. Fateeva, Y. Guo, B. Coasne and D. Farrusseng, *Chem. Soc. Rev.*, 2014, **43**, 5594–5617.
3 M. Ding, X. Cai and H.-L. Jiang, *Chem. Sci.*, 2019, **10**, 10209–10230.
4 J. A. Mason, J. Oktawiec, M. K. Taylor, M. R. Hudson, J. Rodriguez, J. E. Bachman, M. I. Gonzalez, A. Cervellino, A. Guagliardi, C. M. Brown, P. L. Llewellyn, N. Masciocchi and J. R. Long, *Nature*, 2015, **527**, 357–361.
5 T. He, X.-J. Kong, Z.-X. Bian, Y.-Z. Zhang, G.-R. Si, L.-H. Xie, X.-Q. Wu, H. Huang, Z. Chang, X.-H. Bu, M. J. Zaworotko, Z.-R. Nie and J.-R. Li, *Nat. Mater.*, 2022, **21**, 689–695.
6 G.-D. Wang, R. Krishna, Y.-Z. Li, W.-J. Shi, L. Hou, Y.-Y. Wang and Z. Zhu, *Angew. Chem., Int. Ed.*, 2022, **61**, e202213015.
7 F. Niekiel, J. Lannoeye, H. Reinsch, A. S. Munn, A. Heerwig, I. Zizak, S. Kaskel, R. I. Walton, D. de Vos, P. Llewellyn, A. Lieb, G. Maurin and N. Stock, *Inorg. Chem.*, 2014, **53**, 4610–4620.
8 S. Navalón, A. Dhakshinamoorthy, M. Álvaro, B. Ferrer and H. García, *Chem. Rev.*, 2023, **123**, 445–490.

9 N.-Y. Huang, H. He, H. Li, P.-Q. Liao and X.-M. Chen, *Chem. Commun.*, 2020, **56**, 6700–6703.
10 J. Li, C. Wang, D. Wang, C. Yang, X. Cui, X. J. Gao and Z. Zhang, *J. Mater. Chem. A*, 2022, **10**, 20018–20023.
11 W.-B. Li, Y. Wu, X.-F. Zhong, X.-H. Chen, G. Liang, J.-W. Ye, Z.-W. Mo and X.-M. Chen, *Angew. Chem., Int. Ed.*, 2023, **62**, e202303500.
12 H. Guo, S. Su, Y. Liu, X. Ren and W. Guo, *Environ. Sci. Pollut. Res.*, 2020, **27**, 17194–17204.
13 Q. Yan, X. Duan, Y. Liu, F.-Y. Ge and H. Zheng, *J. Mater. Chem. A*, 2023, **11**, 1430–1438.
14 Y. Kong, C. Lu, J. Wang, S. Ying, T. Liu, X. Ma and F.-Y. Yi, *Inorg. Chem.*, 2022, **61**, 10934–10941.
15 J. Shen, R. Kortlever, R. Kas, Y. Y. Birdja, O. Diaz-Morales, Y. Kwon, I. Ledezma-Yanez, K. J. Schouten, G. Mul and M. T. Koper, *Nat. Commun.*, 2015, **6**, 8177.
16 Q. Wang, W.-J. Zhou, S. Heyte, J. Thuriot-Roukos, M. Marinova, A. Addad, S. Rouzière, P. Simon, M. Capron and V. V. Ordomsky, *Chem. Mater.*, 2021, **33**, 8501–8511.
17 L. Zhu, X.-Q. Liu, H.-L. Jiang and L.-B. Sun, *Chem. Rev.*, 2017, **117**, 8129–8176.
18 A. Bavykina, N. Kolobov, I. S. Khan, J. A. Bau, A. Ramirez and J. Gascon, *Chem. Rev.*, 2020, **120**, 8468–8535.
19 X.-J. Kong, T. He, Y.-Z. Zhang, X.-Q. Wu, S.-N. Wang, M.-M. Xu, G.-R. Si and J.-R. Li, *Chem. Sci.*, 2019, **10**, 3949–3955.
20 G. Han, F. Li, M. Guo, H. Fan, Q. Guo and G. Yu, *Chem. Eng. J.*, 2023, **471**, 144545.
21 H. Lyu, O. I. Chen, N. Hanikel, M. I. Hossain, R. W. Flaig, X. Pei, A. Amin, M. D. Doherty, R. K. Impastato, T. G. Glover, D. R. Moore and O. M. Yaghi, *J. Am. Chem. Soc.*, 2022, **144**, 2387–2396.
22 M. Kim and S. M. Cohen, *CrystEngComm*, 2012, **14**, 4096–4104.
23 T. He, X.-J. Kong, J. Zhou, C. Zhao, K. Wang, X.-Q. Wu, X.-L. Lv, G.-R. Si, J.-R. Li and Z.-R. Nie, *J. Am. Chem. Soc.*, 2021, **143**, 9901–9911.
24 M.-M. Xu, Q. Chen, L.-H. Xie and J.-R. Li, *Coord. Chem. Rev.*, 2020, **421**, 213421.
25 F. Zhang, Y. Zhang, X. Wang, J. Li and J. Yang, *Inorg. Chem. Front.*, 2022, **9**, 5434–5443.
26 K. Wang, Y. Li, L.-H. Xie, X. Li and J.-R. Li, *Chem. Soc. Rev.*, 2022, **51**, 6417–6441.
27 J.-K. Jin, K. Wu, X.-Y. Liu, G.-Q. Huang, Y.-L. Huang, D. Luo, M. Xie, Y. Zhao, W. Lu, X.-P. Zhou, J. He and D. Li, *J. Am. Chem. Soc.*, 2021, **143**, 21340–21349.
28 Y.-Z. Zhang, T. He, X.-J. Kong, Z.-X. Bian, X.-Q. Wu and J.-R. Li, *ACS Mater. Lett.*, 2019, **1**, 20–24.
29 C. Pettinari, A. Tăbăcaru and S. Galli, *Coord. Chem. Rev.*, 2016, **307**, 1–31.
30 K. Wang, X.-L. Lv, D. Feng, J. Li, S. Chen, J. Sun, L. Song, Y. Xie, J.-R. Li and H.-C. Zhou, *J. Am. Chem. Soc.*, 2016, **138**, 914–919.
31 D. J. Xiao, M. I. Gonzalez, L. E. Darago, K. D. Vogiatzis, E. Haldoupis, L. Gagliardi and J. R. Long, *J. Am. Chem. Soc.*, 2016, **138**, 7161–7170.
32 N.-Y. Huang, J.-Q. Shen, Z.-M. Ye, W.-X. Zhang, P.-Q. Liao and X.-M. Chen, *Chem. Sci.*, 2019, **10**, 9859–9864.
33 V. Colombo, S. Galli, H. J. Choi, G. D. Han, A. Maspero, G. Palmisano, N. Masciocchi and J. R. Long, *Chem. Sci.*, 2011, **2**, 1311–1319.
34 A. Coelho, *J. Appl. Crystallogr.*, 2018, **51**, 210–218.
35 N. Selvam, S. J. Kwak, G. H. Choi, M. J. Oh, H. Kim, W.-S. Yoon, W. B. Lee and P. J. Yoo, *ACS Energy Lett.*, 2021, **6**, 4345–4354.
36 X.-F. Lu, P.-Q. Liao, J.-W. Wang, J.-X. Wu, X.-W. Chen, C.-T. He, J.-P. Zhang, G.-R. Li and X.-M. Chen, *J. Am. Chem. Soc.*, 2016, **138**, 8336–8339.